Ultrasonics - Sonochemistry 58 (2019) 104621

Contents lists available at ScienceDirect

Ultrasonics - Sonochemistry

journal homepage: www.elsevier.com/locate/ultson

Sonochemical synthesis of Eu^{3+} substituted $CoFe_2O_4$ nanoparticles and their structural, optical and magnetic properties

M.A. Almessiere[a,b], Y. Slimani[a,*], A.D. Korkmaz[c], N. Taskhandi[d], M. Sertkol[e], A. Baykal[d], Sagar E. Shirsath[f], İ. Ercan[a], B. Ozçelik[g]

[a] Department of Biophysics, Institute for Research & Medical Consultations (IRMC), Imam Abdulrahman Bin Faisal University, P.O. Box 1982, 31441 Dammam, Saudi Arabia
[b] Department of Physics, College of Science, Imam Abdulrahman Bin Faisal University, P.O. Box 1982, 31441 Dammam, Saudi Arabia
[c] Department of Chemistry, Istanbul Medeniyet University, 34700 Istanbul, Uskudar, Turkey
[d] Department of Nano-Medicine Research, Institute for Research & Medical Consultations (IRMC), Imam Abdulrahman Bin Faisal University, P.O. Box 1982, 31441 Dammam, Saudi Arabia
[e] Deanship of Preparatory Year, Imam Abdulrahman Bin Faisal University, P.O. Box 1982, 31441 Dammam, Saudi Arabia
[f] School of Materials Science and Engineering, University of New South Wales, Kensington, Sydney, NSW 2052, Australia
[g] Department of Physics, Faculty of Science and Letters, Cukurova University, 01330 Balcali, Adana, Turkey

ARTICLE INFO

Keywords:
Spinel ferrites
Structure
Electron microscopy
Optical properties
Magnetic properties

ABSTRACT

Magnetic, optic and microstructural properties of ultrasonically synthesized $CoEu_xFe_{2-x}O_4$ ($x \leq 0.1$) nanoferrites (NFs) have been examined in this study. After sonochemical synthesis, XRD and FT-IR analyses confirmed the purity, the structure (cubic spinel structure and Fd3m space group) and the spectral properties of the spinel ferrite samples. The spherical morphology and chemical compositions of the products were observed via transmission and scanning electron microscopes along with EDX and elemental mapping. Percent diffuse reflectance (%DR) was used for optical investigation. Optical band gaps (E_g) were estimated utilizing Kubelka-Munk theory and Tauc equation. E_g values are in a narrow band of 1.34 to 1.44 eV. The magnetic parameters like M_s (saturation magnetization), SQR = M_r/M_s (squareness ratio), n_B (magnetic moment), H_c (coercivity) and M_r (remanence) have been evaluated by analyzing measurements of magnetization versus magnetic field performed at room (RT; T = 300 K) and low (T = 10 K) temperatures. It is showed that the different produced $CoEu_xFe_{2-x}O_4$ ($0.00 \leq x \leq 0.10$) nanospinel ferrites present superparamagnetic (SPM) nature at RT. At low temperature, the various produced $CoEu_xFe_{2-x}O_4$ ($x \leq 0.08$) nanospinel ferrites display ferrimagnetic (FM) nature. With exception, the x = 0.10 sample exhibit SPM behavior at T = 10 K. It is noticed that the Eu^{3+} substitutions alter in a significant way on the magnetic data. A decreasing trend in the M_s, M_r and n_B values was noted with Eu^{3+} substitutions.

1. Introduction

Spinel ferrites have been widely used materials in technological applications as well as in numerous other fields owing to their unique magnetic, optical, and electric properties including low dielectric loss, high magnetization, and a high band gap, etc. [1,2]. These properties can be tuned to obtain materials with different features. Although there are many different types of synthesis approaches for spinel ferrites (co-precipitation, thermal decomposition, polyol method, hydrothermal synthesis, sol-gel auto combustion, microwave routes, etc. [3,4]), the ultrasonication approach has proved to be a timesaving method to obtain high-purity products in a facile way. When compared with other traditional methods, ultrasonication offers minimum waste production, conservation of energy and enhanced rate of reaction. In our work, we applied ultrasonication to obtain nanomaterials. In sonochemical synthesis, during ultrasound irradiation, sound waves propagate through the liquid and at the same time microbubbles are created. These microbubbles receive energy and undergo rapid inertial overgrowth until they implode inward catastrophically through a series of stages collectively referred as cavitation [5]. Within a microsecond, the cavitation bubble collapse occurs and creates local 'hot spots' with a generation of high local temperature and pressure, which fuel the homolysis of water in the system [6,7].

Rare earth (RE) metals offer opportunity to develop novel magnetic

* Corresponding author.
E-mail address: yaslimani@iau.edu.sa (Y. Slimani).

https://doi.org/10.1016/j.ultsonch.2019.104621
Received 3 May 2019; Received in revised form 24 May 2019; Accepted 28 May 2019
Available online 29 May 2019

nanoparticles with new properties. The doping of ferrites with a rare earth element offers an increase in the magnetic characteristics as well as in electrical and structural features [8]. Two classes of rare earth ions exist: the ones whose radii are greater than that of iron ions and the ones with radii smaller than the radius of iron ions [9]. When there is a greater difference in ionic radii, micro-strains will be formed within the structure. This may cause domain wall motion that in turn causes a deformation into the spinel lattice. The inclusion of RE ions into the ferrites structure results in the substitution of iron (III) ions with the larger rare earth metallic ions to reside in the octahedral sites, which may induce limited solubility in the spinel lattice structure. As it is known, there are unpaired electrons in the 4f orbitals of rare earth metals, which possess strong spin-orbit couplings of the angular momentum compared to the 3d transition metals [10]. The interaction between the rare earth ion and ferrite ion occurs through 4f-3d coupling [11]. This exchange coupling determines the magneto-crystalline anisotropy and hence can result in changes in Curie temperature, magnetic properties, electric characteristics as well as catalytic properties of ferrites [12].

The substitution of iron with rare earth elements was investigated by several different researchers. Various groups investigated the magnetic characteristics of ferrites substituted with rare earth ions. Co-Zn ferrite nanoparticles were substituted by dysprosium in a study by Kulal [13]. Kabbur et al. investigated the effect of Tb^{3+} introduction to Ni-CuZn ferrites. They found the incorporation of Terbium (III) ions in $Ni_{0.25}Cu_{0.30}Zn_{0.45}Tb_xFe_{2-x}O_4$ ferrites caused a decrease in Ms as well as Curie temperature [14]. Another group also synthesized Erbium (III) substituted $CoFe_2O_4$ NPs and investigated their magnetic properties. The Ms decreased, and the particle size slightly decreased as the amount of Er^{3+} content increased [15]. Zubair et al. [16] examined the magnetic, structural and morphological properties of Eu doping $CoFe_2O_4$ nano-ferrites and they found out that magnetic behavior is strongly dependent on Eu addition.

Ferrite nanoparticles incorporated with rare earth ions also display potential optical applications. Several research groups have focused on the optical investigation of rare earth metal substituted nano-sized ferrites. Nasrabadi et al. [17] prepared copper ferrite nanoparticles doped with Ce^{3+} with sol-gel auto combustion and studied the optical characteristics of obtained $CuFe_{2-x}Ce_xO_4$ nanoparticles. When they calculated the band gap with Tauc equation, they determined the band gap (E_g) value 2.8 eV and applied the doped-ferrite NPs as photocatalysts for the degradation of methyl orange. Lanthanum (III) was employed as a dopant for $ZnFe_2O_4$ nanoparticles in another study [18]. The optical band gap (E_g) increased from 1.87 eV for x = 0.0 (zinc ferrite) to 1.97 eV for x = 0.06 in $ZnFe_{2-x}La_xO_4$ (x = 0.00, 0.02, 0.04, 0.06) NPs. The excellent absorption band of Gd^{3+}-doped zinc ferrites in visible spectrum showed potential applications for $ZnFe_{2-x}La_xO_4$ nanoparticles (NPs). The same group also examined the impact of Er^{3+} substitutions on magnetic, structure and optical characteristics of magnesium ferrite NPs with a formula $MgFe_{2-x}Er_xO_4$ (x = 0, 0.02, 0.04, and 0.06) [19]. As the amount of Erbium (III) increased, the synthesized products displayed higher E_g (ranging from 1.91 to 1.96 eV compared to 1.81 in undoped NPs). They concluded that this is owing to the greater ionic radii (1.004 Å) of Er^{3+} ions in comparison to Fe^{3+} ions (0.645 Å). Recently, our group has evaluated the substitution of iron (III) with three different rare earth ions (Ce, Dy, and Y) in Co-Zn ferrites $Co_{0.5}Zn_{0.5}Fe_{2-x}RE_xO_4$ ($0.00 \le x \le 0.05$) [20].

In this study, we synthesized Eu^{3+} substituted copper ferrite nanoparticles, $CoEu_xFe_{2-x}O_4$ ($x \le 0.1$) NPs, with a sonochemical-assisted approach. The structure, magnetic, and optical properties of prepared NPs were examined by XRD, FT-IR, FE-SEM/EDX, VSM, and diffuse reflectance spectroscopy methods. The goal is to investigate the effect of Eu^{3+} substitution on structural, optical and magnetic properties cobalt ferrite NPs.

2. Experimental procedure

Sonochemical technique was utilized to fabricate $CoEu_xFe_{2-x}O_4$ ($0.0 \le x \le 0.1$) NFs. A precise ratios of $Co(NO_3)_2{\cdot}6H_2O$ (cobalt nitrate hexahydrate), $Fe(NO_3)_3{\cdot}9H_2O$ (Iron (III) nitrate nonahydrate) are thawed with 80 ml of deionized water (DI H_2O) under vigorous stirring and the stoichiometric amounts Europium (III) oxide (Eu_2O_3) in 15 ml of concentration HCl. Subsequently, both solutions are mixed together and adjusted the pH at 11 by using NH_3 solution. Lastly, the solution will setted up under the ultrasonic irradiation with high-intensity (20 kHz frequency and 70 W power, (UZ SONOPULS HD 2070) for 30 min. As a result, the mixture temperature reached out 90 °C when the ultrasonication process ended. The resultant powder washed with the mixture of DI H_2O and ethanol (50% v/v) and then the solid product was divided from the liquid with centrifuged and dried at 100 °C for 3 h.

Phase identification has been proceeded through Rigaku Benchtop Miniflex XRD with CuKα radiation. The surface analysis was performed by SEM (FEI Titan ST) coupled with EDX system and TEM (FEI Morgagni 268). FT-IR (Bruker) spectra were registered via a spectrometer over the wavelength range 4000–400 cm^{-1}. UV–visible diffuse reflectance (DR%) spectra were obtained in the 200–800 nm wavelength range using a DR spectrophotometer. The magnetization measurements have been executed by a Quantum Design PPMS with vibrating sample magnetometer (VSM) head.

3. Results and discussion

3.1. Crystal structure and cation distribution

Fig. 1 represented XRD patterns of $CoEu_xFe_{2-x}O_4$ ($x \le 0.1$) NFs. All

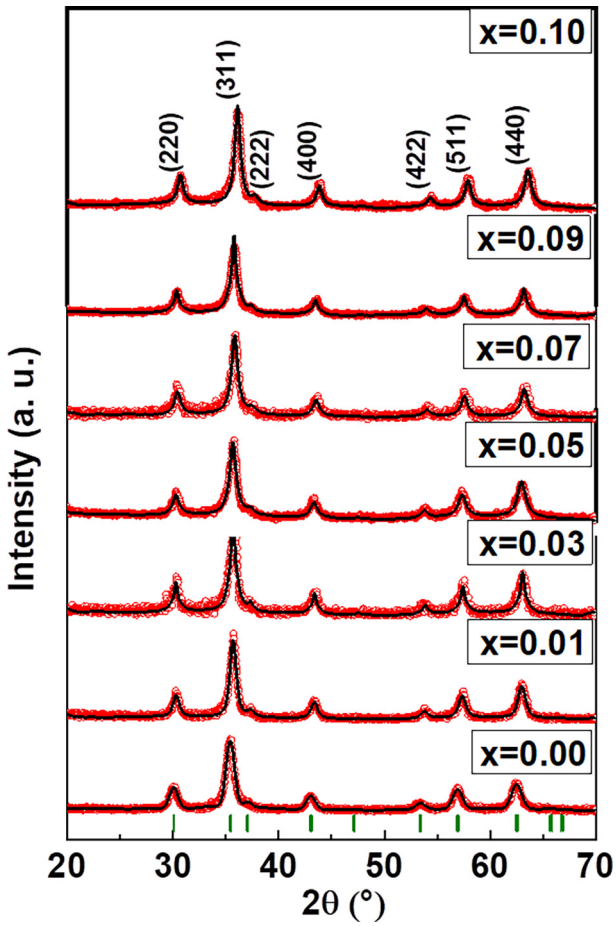

Fig. 1. XRD powder patterns of $CoEu_xFe_{2-x}O_4$ ($x \le 0.1$) NFs.

Table 1
Refined structural parameters, crystallites size and magnetic particles size of $CoEu_xFe_{2-x}O_4$ (x ≤ 0.1) NFs.

x	a (Å)	V (Å)^3	χ^2 (chi^2)	R_{Bragg}	D_{XRD} (nm) ± 0.05	D_M (nm)
0.00	8.3563	583.50	2.23	17.70	11.1	10.5
0.01	8.3469	581.53	2.28	10.60	15.1	14.0
0.03	8.3420	580.50	2.65	18.37	23.9	20.4
0.05	8.3396	580.01	1.93	18.4	16.3	14.8
0.07	8.3266	577.29	2.27	15.62	15.5	13.9
0.09	8.3228	576.51	0.90	9.10	24.8	20.7
0.10	8.3115	574.16	0.77	9.49	19.7	15.3

ratios of Eu substituted Co-ferrite showed the characteristic peaks of spinel ferrite without any impurity. This is an evident that the Eu well-cooperated into the spinel crystal and does not change the cubic structure by only using sonication as preparation methods without calcination. The lattice constants and average crystallite size are estimated through Rietveld refinement by full proof for all XRD experimental data as given in Table 1. The lattice constant "a" was found to decrease with increasing the Eu content, which is due to the iron vacancies through the crystallization by Eu lead to shrink the lattice. Similar results have been reported in the literature [21,22]. Moreover, the average crystallites size (D_{XRD}) is calculated by Debye–Scherrer formula of (3 1 1) peak and it found in the range from 11 to 24 nm as tableted in Table 1 [23–25].

Since the magnetic and structural properties of ferrites are greatly cation distribution dependent, Bertaut method based on XRD pattern analysis was employed to estimate the cation distribution in $CoEu_xFe_{2-x}O_4$ ferrite system [26]. It is known that the divalent and trivalent cations distribution among the O_h and T_d crystallographic sites was determined from the ratio of the intensity of I_{220}/I_{440} and I_{422}/I_{400} planes [27]. The cations exhibit nearly linear composition and substitution dependencies (Table 2). Fe^{3+} and Co^{2+} ions occupied O_h and T_d crystallographic sites. According to the single-ion model, the fully inverse spinel structure Co^{2+} are expected to occupy octahedral B site [28,29], however in the present case the prepared samples are considered as random spinel since Co^{2+} ions occupied both the sites. Percentage of Fe^{3+} ions at the O_h site decreased with increasing Eu^{3+} substitution.

3.2. Infrared investigation

FT-IR spectra of $CoEu_xFe_{2-x}O_4$ (x ≤ 0.1) NFs are displayed in Fig. 2. Samples exhibited the two prominent vibration bands of spinel ferrite at 588.14 and 398.08 cm^{-1} that denoted metal-oxygen bond vibration of the tetrahedral and octahedral lattices [30–32]. The vibration bands are shifted to higher wavenumber because of the reduction in bond length, strength and broadening with increasing the Eu content of the tetrahedral and octahedral sites [20,33,34].

3.3. Morphological investigation

FE-SEM images of $CoEu_xFe_{2-x}O_4$ (x ≤ 0.1) NFs are presented in Fig. 3. FE-SEM images revealed an agglomeration of grains due to the magnetic interactions. The grains size is less than 20 nm for various compositions, which is in agreement with XRD results. EDX and elemental mapping were carried out the selected x = 0.03 and 0.07 compositions (Fig. 4). They showed the existence of the different constituent elements Co, Eu, Fe and O. The chemical compositions (Insets of Fig. 4) proved the formation of the desired compositions. Fig. 5 depicted the TEM images of the x = 0.05 composition. TEM image indicated a high aggregation of nanoparticles with average size smaller than 20 nm. Moreover, the selected area electron diffraction (SAED) pattern shows continuous spots and separated rings, indicating that the nanoparticles are well crystallized. The observed rings are associated to the crystalline structure of Co spinel ferrite.

Table 2
Cation distribution of $CoEu_xFe_{2-x}O_4$ (x ≤ 0.1) NFs based on the Rietveld method.

x	Tetrahedral A-site	Octahedral B-site
0.00	$Co_{0.15}Fe_{0.85}$	$Co_{0.85}Fe_{1.15}$
0.01	$Co_{0.2}Fe_{0.8}$	$Co_{0.8}Eu_{0.01}Fe_{1.19}$
0.03	$Co_{0.2}Fe_{0.8}$	$Co_{0.8}Eu_{0.03}Fe_{1.17}$
0.05	$Co_{0.2}Fe_{0.8}$	$Co_{0.8}Eu_{0.05}Fe_{1.15}$
0.07	$Co_{0.2}Fe_{0.8}$	$Co_{0.8}Eu_{0.07}Fe_{1.13}$
0.09	$Co_{0.21}Fe_{0.79}$	$Co_{0.79}Eu_{0.09}Fe_{1.12}$
0.10	$Co_{0.22}Fe_{0.78}$	$Co_{0.78}Eu_{0.1}Fe_{1.12}$

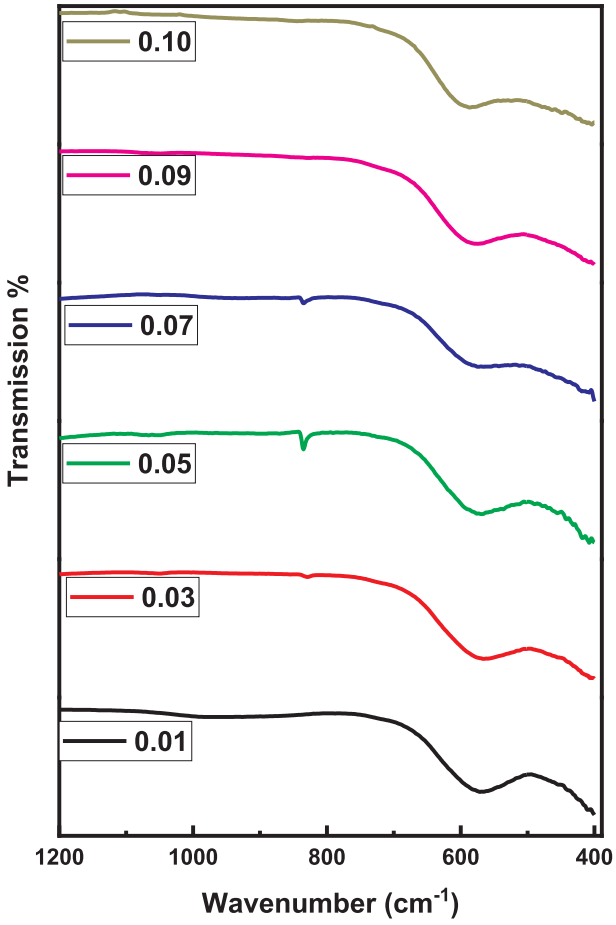

Fig. 2. FT-IR spectra of $CoEu_xFe_{2-x}O_4$ (x ≤ 0.1) NFs.

3.4. Optical study

Magneto optical properties of $CoEu_xFe_{2-x}O_4$ (x ≤ 0.1) NFs were specified via UV–Visible DRS studies. DR% measurements were performed in a wavelength region of 200–800 nm (Fig. 6). Photon energies of 1.55 eV and 6.2 eV correspond to 800 nm and 200 nm wavelengths of applied radiation, respectively. Recorded spectra have reflectance intensities in a narrow band of 12–20% in the near UV and visible regions of electromagnetic radiation.

The analyses of recorded spectra are based on Kubelka-Munk function, $F(R_\infty)$ [35–37]:

$$F(R_\infty) = \frac{(1-R_\infty)^2}{2R_\infty} = \frac{2.303\varepsilon C}{S} = \alpha \quad (1)$$

where R_∞ is reflectance of infinitely thick sample, ε is absorptivity, S is effective scattering coefficient, C is analyte concentration and α is

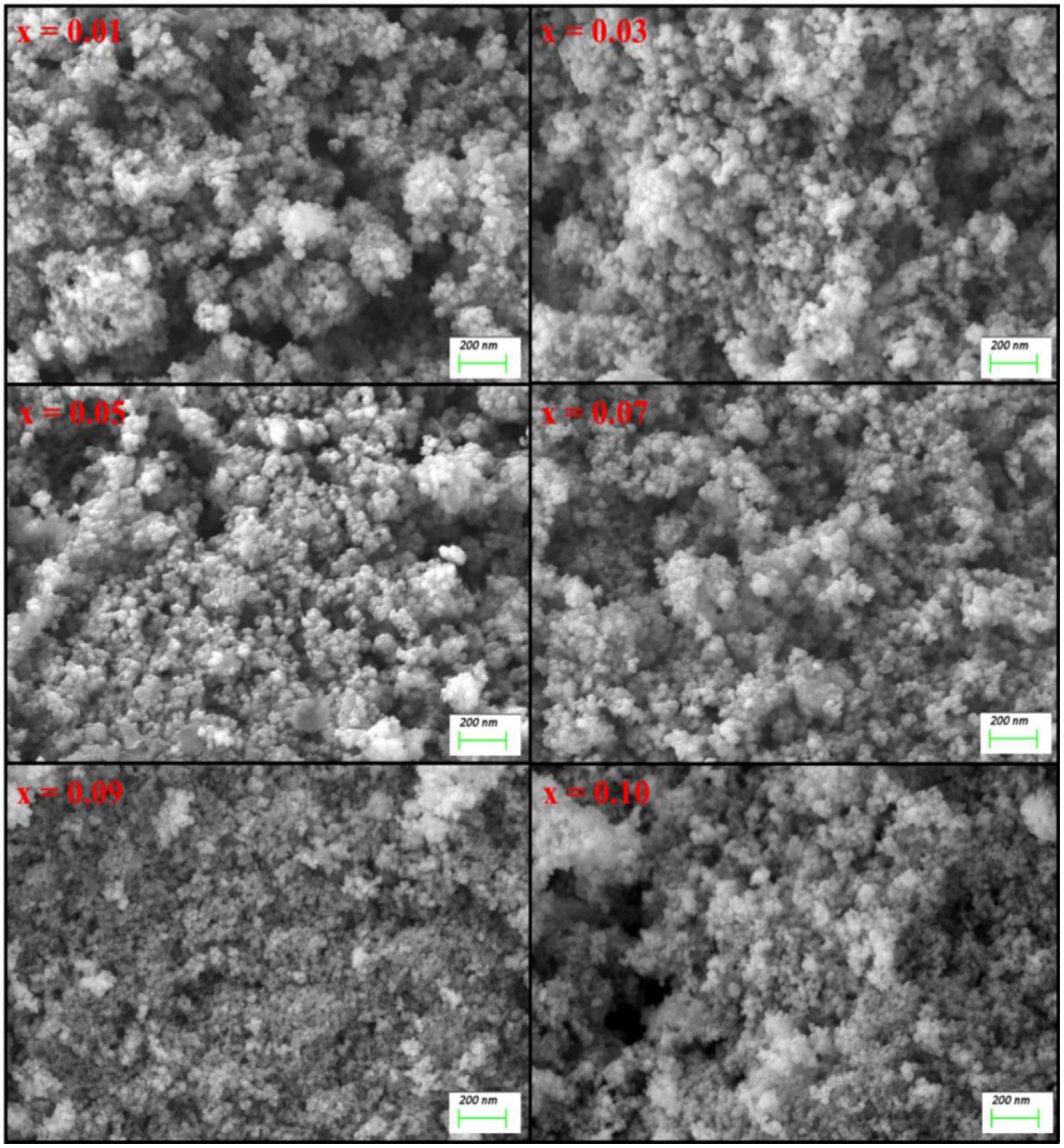

Fig. 3. FE-SEM images of $CoEu_xFe_{2-x}O_4$ ($x \leq 0.1$) NFs.

absorption coefficient. Optical band gap (E_g) of samples are evaluated applying Tauc equation that correlates the absorption coefficient and E_g [35–37] as below:

$$(\alpha h\upsilon)^n = A(h\upsilon - E_g) \quad (2)$$

where A is a proportionality constant, ($h\upsilon$) is the incident photon energy, and the power n denotes the type of electronic transition. For instance, power $n = 1/2$ denotes an indirect-allowed electronic transition. A straight line from the upper part of $(\alpha h\upsilon)^n$ versus ($h\upsilon$) graph intercepts the energy axis at $(\alpha h\upsilon)^n = 0$, then the corresponding value energy axis is assigned as optical energy band gap. Fig. 7 includes the Tauc plots and estimated band gaps for all samples. All Tauc plots have y-axis of $(\alpha h\upsilon)^2$ which means that the power equals to 2 and assign direct-allowed transitions for all pristine and doped samples. Pristine $CoFe_2O_4$ has 1.34 eV band gap magnitude. When this magnitude is compared with doped samples, one can easily say that Eu^{3+} ion causes slight increments at direct E_g magnitudes within the x = 0.03 or higher ion dope ratios. $CoEu_{0.05}Fe_{1.95}O_4$ has maximum band gap of 1.44 eV. All estimated data can be accepted to lie in the semiconductor band gap range. In the literature, there are reported direct or indirect E_g data for pristine and doped $CoFe_2O_4$ NPs with the ions of different elements Zn, Ni, Y, Nb except Eu [38–45]. Those report the direct or indirect allowed transition values in a wide range of 0.48–4.3 eV. Our data and reported direct optical E_g values by Quinonez and co-workers [44] accord very well.

3.5. Magnetization analyses

M-H loops for all $CoEu_xFe_{2-x}O_4$ ($x \leq 0.10$) NFs performed at RT and 10 K are presented in Figs. 8 and 9, respectively. It is obvious that the Eu^{3+} substitutions in the Fe^{3+} sites affect significantly the magnetic properties of Co spinel ferrite. Stoner–Wohlfarth (S–W) approach was utilized to extract M_s values as reported in the references [46–48]. The deduced magnetic parameters M_s, M_r and H_c are plotted in the Fig. 10. At RT (T = 300 K), the magnitudes of M_s are ranging between 20.8 and 49.2 emu/g. The considered M_r and H_c values of various products are negligible at RT. Accordingly, one can establish that the $CoEu_xFe_{2-x}O_4$ ($x \leq 0.10$) NFs present superparamagnetic (SPM) nature at RT. The M-H behavior in the superparamagnetic state can be correlated with the Langevin function that takes into account a Boltzman distribution of the energy level corresponding to all of the possible orientations of the particle magnetization moment [49,50]:

$$M(H) = M(\infty)L(x) \quad (3)$$

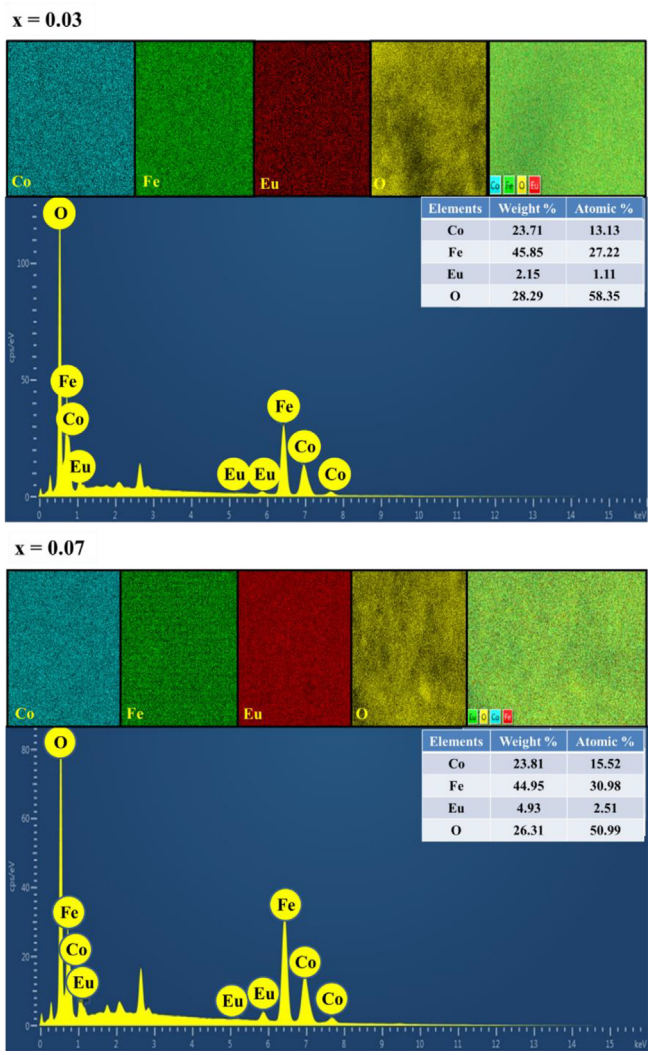

Fig. 4. EDX spectra and elemental mapping images of $CoEu_xFe_{2-x}O_4$ (x = 0.03 and 0.07) NFs.

where $M(H)$ is the magnetization versus field, $M(\infty)$ is the magnetization at saturation, and L(x) is the Langevin function [49,50]:

$$L(x) = [\coth(x) - 1/x] \text{with} x = \frac{M_s VH}{k_B T} \quad (4)$$

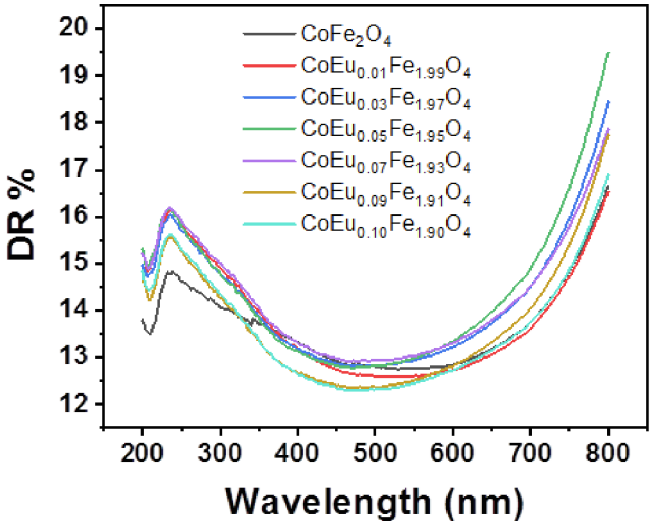

Fig. 6. DR% spectra of $CoEu_xFe_{2-x}O_4$ (x ≤ 0.1) NFs.

The volume of spherical particles $V = \frac{\pi D_M^3}{6}$. The fitting of the experimental magnetization curves (Fig. 8) by Eqs. (3) and (4) allows the determination of the size of magnetic nanoparticles D_M. The deduced values of D_M are listed in Table 1. It can be seen (Table 1) that the D_M values were smaller than the D_{XRD} ones. This is mostly due to magnetic dead layer on the top of crystalline core. The non-magnetic surface layer of the nanoparticles usually results in a smaller magnetic size than the physical size [50]. At low temperatures (T = 10 K), various nanospinel ferrites showed M_s values ranging between 26.6 and 62.9 emu/g. Fig. 9(b) shows detailed hysteresis loops at T = 10 K to make the coercivity visible. Except the composition x = 0.10, an hysteresis was clearly noticed for the other various products at 10 K. Therefore, the various produced $CoEu_xFe_{2-x}O_4$ (0.00 ≤ x ≤ 0.08) nanospinel ferrites present hard ferrimagnetic (FM) nature at 10 K. Nevertheless, the composition x = 0.10 exhibit SPM behavior. It is obvious in Fig. 9(b) that the hysteresis loops at T = 10 K showed a "wasp-waisted" or "kink" behavior, which is not noticed at RT. For such kind of loops, numerous explanations have been described such as the magnetic coupling among the various magnetic phases having dissimilar coercivities and/or the re-ordering of the magnetic spins at lower temperatures under the effect of the applied field [51,52]. The re-orientation of spins is responsible for controlled on M(H) loops that could be described by taking into account the motion of domain walls and the pinning of the potential wells produced by the directional order [51,53]. This modifies the magnetic properties of the products. The

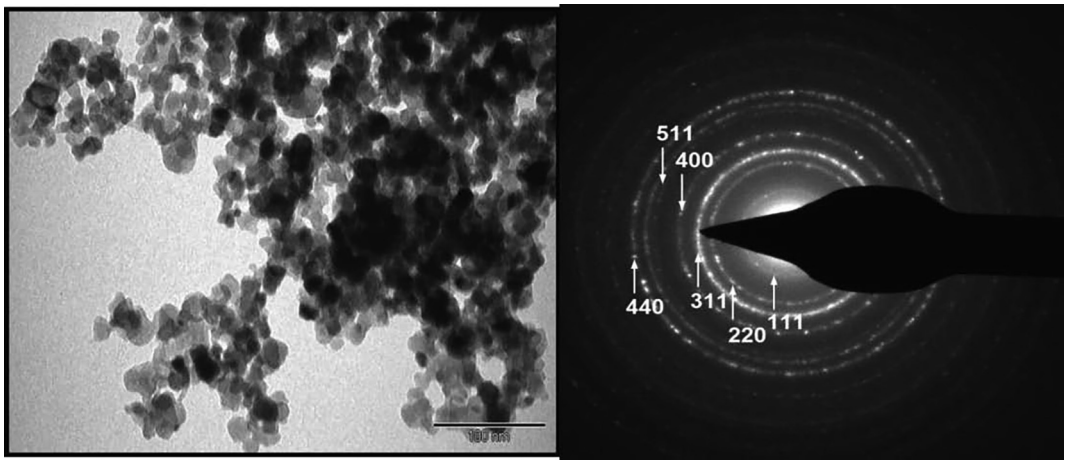

Fig. 5. TEM and SEAD images of $CoEu_xFe_{2-x}O_4$ (x = 0.05) NF.

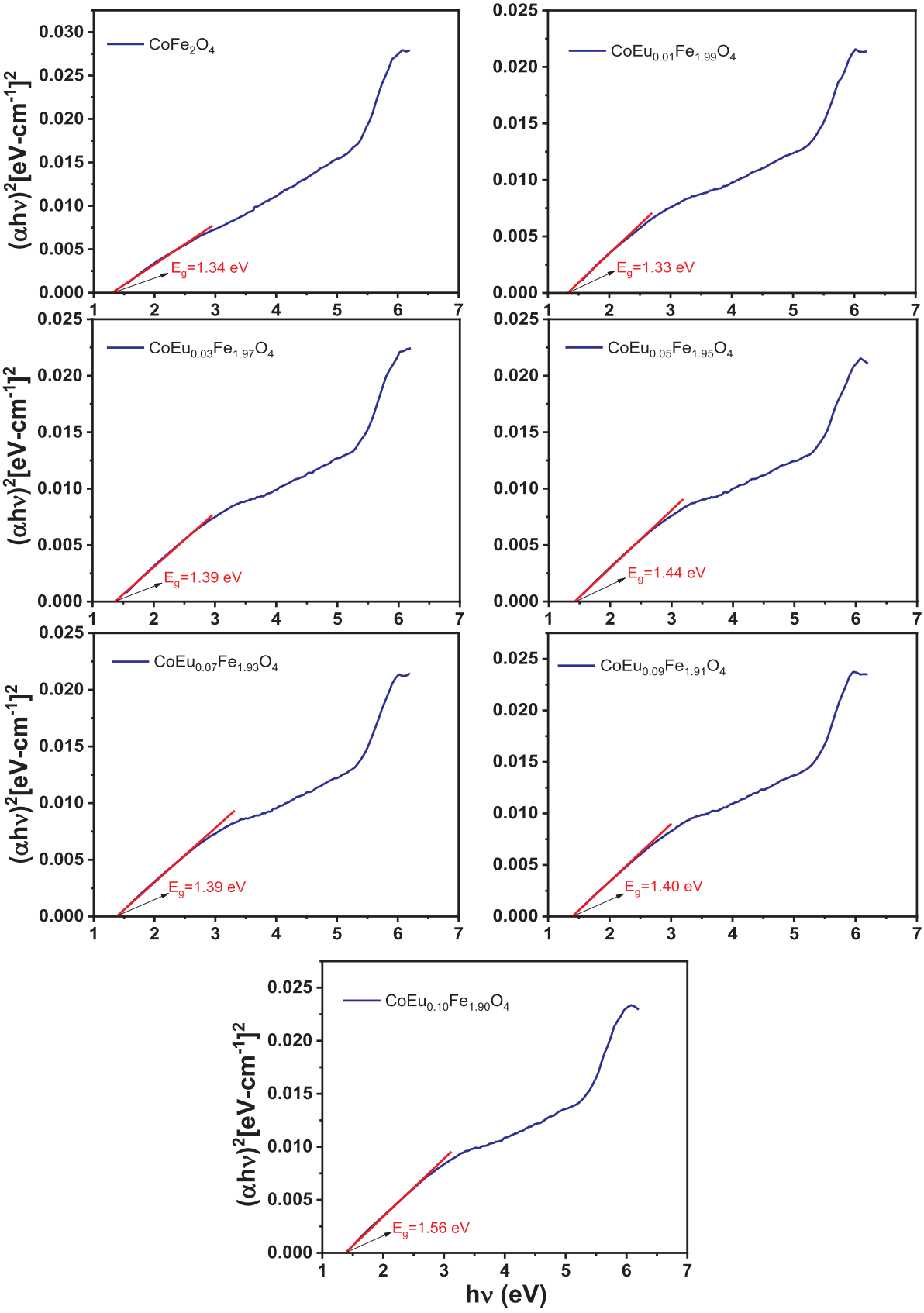

Fig. 7. Tauc plots of $CoEu_xFe_{2-x}O_4$ ($x \leq 0.1$) NFs. Extrapolating the straight portion of the plot to the photon energy axis at the $(\alpha h\upsilon)^2 = 0$ determines the value of optical band gap.

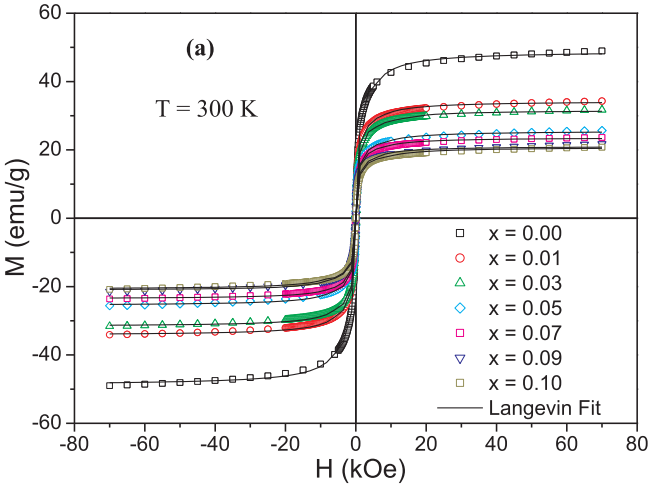

Fig. 8. Magnetization versus applied magnetic field, M(H), measured at RT for $CoEu_xFe_{2-x}O_4$ ($x \leq 0.10$) NFs. The solid lines represent the Langevin fit.

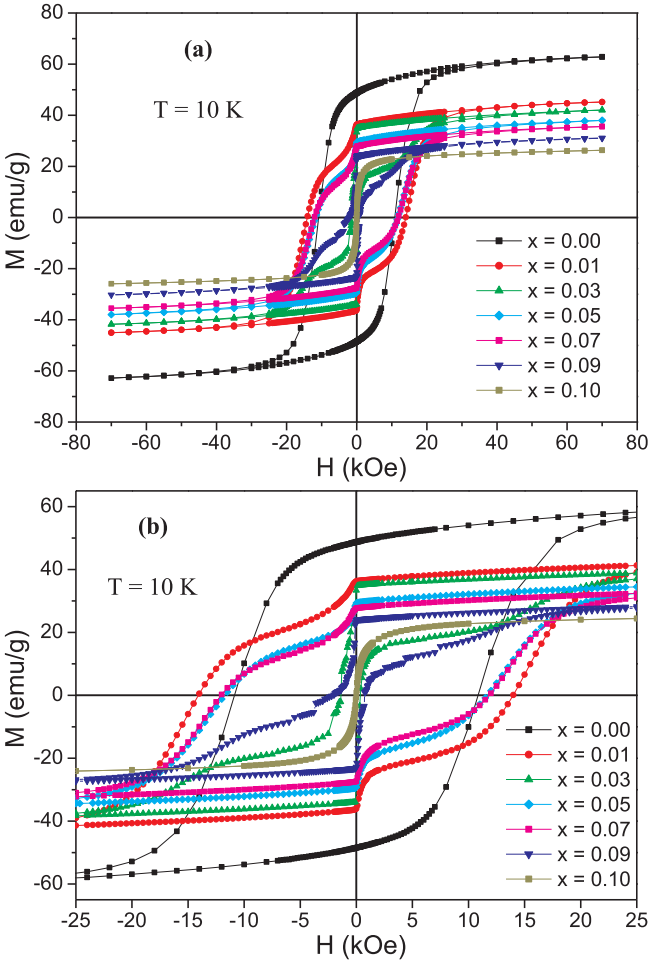

Fig. 9. (a) M(H) hysteresis loops carried out at 10 K for $CoEu_xFe_{2-x}O_4$ ($x \leq 0.10$) NFs. (b) An enlarged view of M(H) loops for H ranging between −25 and +25 kOe.

oxidation of soft magnetic layers in the occurrence of atmospheric oxygen could be another plausible cause [51,54]. Such kind of comportment results from the combination of grain boundaries and mixture of magnetic composites exhibiting dissimilar magnetic characteristics [51,55]. In the current study, it is assumed that the "kink" behavior in M-H loops could be caused by the occurrence of Co (hard) and Eu (soft)

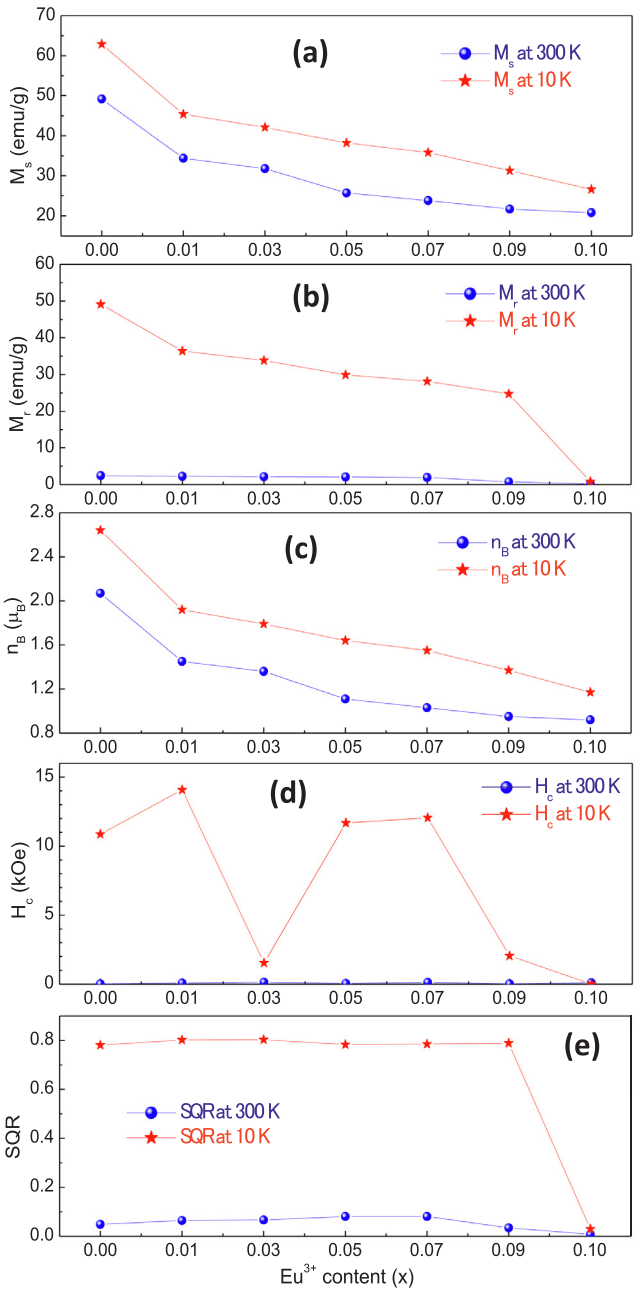

Fig. 10. Evolutions of (a) M_s, (b) M_r, (c) n_B, (d) H_c and (e) SQR versus Eu^{3+} substitution content at both RT and 10 K.

phases in the products. On the other hand, one should note that the M-H results showed an increment in M_s, M_r and H_c of various samples when the temperature decreased down from 300 to 10 K. The increasing trend of these magnetic parameters could be explained by taking into account that at lower temperatures the magnetic anisotropy rises and the scatter of particles in the direction of the anisotropic field owing to which the magnetic parameters increase [51,56,57]. In nanoparticles, the influence of thermal fluctuations of blocked moments within the anisotropy barriers is responsible for the improvement in various magnetic parameters at lower temperatures [51,58]. Hence, the reduced thermal fluctuations with reducing the temperature have the capability to render the magnetic moments isotropic, which cause an enhancement in various magnetic parameters of the product [51,59].

Fig. 10 reports the impacts of Eu^{3+} substitution on the M_s, M_r and H_c of various prepared $CoEu_xFe_{2-x}O_4$ NFs. Among various products, the pristine x = 0.00 NF exhibits the maximum M_s values of 49.2 and

62.9 emu/g at RT and 10 K, respectively. The obtained magnitudes are smaller than that for various bulk inverse spinel Co ferrites [60]. The lower M_s compared to that of bulk material is largely accredited to the smaller crystallites size. This leads to structural disorder on the surface for the reason that the spins disorder will be significant when the volume and surface ratio is important [24,25]. The spins canting as a result of antiferromagnetic interactions competition and the disordered cations distribution on the surface could explain the lowering of M_s magnitude [20,25]. On the other hand, the M_s values exhibited a decreasing tendency with increasing the Eu^{3+} substitution content in nanospinel Co ferrite at both measured temperatures. M_s is lowest for product with x = 0.10. Analogous tendency is surveyed in M_r evolution. Compared to x = 0.00 product, M_r showed a decreasing behavior with increasing Eu^{3+} content. Indeed, the evolutions in remanence track principally the evolutions in M_s [61]. In the literature, it is reported that several parameters could alter the magnetic properties of magnetic nanoparticles such as strains, variations in grains size, strength of super-exchange interactions, variations in magnetic moments (n_B), etc [45,62]. Besides, it is known that the Eu^{3+} ions (1.07 Å) have larger radius than that of Fe^{3+} ions (0.645 Å) [63]. The dissimilarity in ionic radii possibly will produce strains and disorder that vary the electronic states and disturb the ferrite systems [25]. On the other hand, the relation between n_B and M_s is given by the following expression [63]:

$$n_B = \frac{Moleculor\ \ Weight\ x\ M_s}{5585} \quad (5)$$

The evolution in n_B values for all concentrations is presented in Fig. 10(c). Frequently, the diminution in n_B values is originating from the weakening in the super-exchange interactions between different sites. Here, the x = 0.00 sample present the extreme n_B and M_s. With the increase in Eu^{3+} concentration, n_B showed a decreasing tendency like that in M_s and M_r cases. These results imply a weakening of super-exchange interactions with Eu^{3+} substitutions in nanospinel Co ferrites. The variation of H_c values versus Eu^{3+} content at RT and 10 K is reported in Fig. 10(d). At RT, the H_c values are negligible, however they are very large at 10 K. At low temperature (T = 10 K), H_c is highest for × = 0.01 product and lowest for × = 0.10 one. Generally, the coercivity is controlled by numerous parameters including the magnetocrystalline anisotropy, morphology, shape and grains size [25,64]. The SQR values at RT and 10 K are also determined and presented in the Fig. 10(e). Generally, it is known that the NPs are in single magnetic domain (SD) when SQR ≥ 0.5 [65]. Nevertheless, they are in multi-magnetic domain (MD) when SQR < 0.5 [66]. According to the obtained SQR values ranging between 0.008 and 0.081 at RT, the various produced nanospinel ferrites could be considered to be in MD nature at RT. On the other hand, the various samples, with exception the composition x = 0.10, exhibit SQR values around greater than 0.5 at 10 K indicating SD nature. The x = 0.10 product display SQR = 0.03 at T = 10 K, reflecting the MD nature in this sample.

4. Conclusion

The impact of Eu^{3+} substitutions on the structure, morphology, optic and magnetic properties of $CoFe_2O_4$ NFs have been presented in this study. No secondary phase wad observed. Both SEM and TEM analyses exposed the formation of nano-crystalline grains with spherical morphology. DR% studies revealed that all estimated direct E_g data varying from 1.34 eV belonging to pristine sample and 1.44 eV belonging to $CoEu_{0.05}Fe_{1.95}O_4$ lie in the semiconductor bandgap range for all samples. E_g values slightly increased due to Eu^{3+} ion doping starting from x = 0.03 ratio. M(H) data were deeply investigated and revealed that the different produced $CoEu_xFe_{2-x}O_4$ (x ≤ 0.10) NFs present superparamagnetic (SPM) nature at RT. At 10 K, the various produced $CoEu_xFe_{2-x}O_4$ NFs with x up to 0.08 present hard ferrimagnetic (FM) nature, however the x = 0.10 one exhibit SPM behavior. The deduced M_s, M_r and n_B magnitudes are found to decrease with increasing Eu^{3+} concentration. The obtained magnetic results are a result of the creation of local strains, the weakening of super-exchange interactions and the decreasing in the magnetic moments (n_B). The obtained SQR values at RT suggest a multi-magnetic domain nature for all products. However, single magnetic domain was noticed at T = 10 K for various samples excepting the composition x = 0.10 that reflects a multi-magnetic domain nature at 10 K.

Acknowledgments

The Institute for Research and Medical Consultations of Imam Abdulrahman Bin Faisal University (Saudi Arabia) is highly acknowledged for providing the supports through the Projects application No. 2019-IRMC-S-1.

Appendix A. Supplementary data

Supplementary data to this article can be found online at https://doi.org/10.1016/j.ultsonch.2019.104621.

References

[1] E. Hema, A. Manikandan, M. Gayathri, M. Durka, S. Arul Antony, B.R. Venkatraman, The role of Mn^{2+}-doping on structural, morphological, optical, magnetic and catalytic properties of spinel $ZnFe_2O_4$ nanoparticles, J. Nanosci. Nanotechnol. 16 (2016) 5929–5943.
[2] K. Elayakumar, A. Manikandan, A. Dinesh, K. Thanrasu, K. Kanmani Raja, R. Thilak Kumar, Y. Slimani, S.K. Jaganathan, A. Baykal, Enhanced magnetic property and antibacterial biomedical activity of Ce^{3+} doped $CuFe_2O_4$ spinel nanoparticles synthesized by sol-gel method, J. Magn. Magn. Mater. 478 (2019) 140–147.
[3] A. Mary Jacintha, A. Manikandan, K. Chinnaraj, S. Arul Antony, P. Neeraja, Comparative studies of spinel $MnFe_2O_4$ nanostructures: structural, morphological, optical, magnetic and catalytic properties, J. Nanosci. Nanotechnol. 15 (2015) 9732–9740.
[4] E. Hema, A. Manikandan, P. Karthika, M. Durka, S. Arul Antony, B.R. Venkatraman, Magneto-optical properties of reusable spinel $Ni_xMg_{1-x}Fe_2O_4$ ($0.0 \leq x \leq 1.0$) nano-catalysts, J. Nanosci. Nanotechnol. 16 (2016) 7325–7336.
[5] K. Muthoosamy, S. Manickam, State of the art and recent advances in the ultrasound-assisted synthesis, exfoliation and functionalization of graphene derivatives, Ultrason. Sonochem. 39 (2017) 478–493.
[6] K.S. Suslick, G.J. Price, Applications of ultrasound to materials chemistry, Annu. Rev. Mater. Sci. 29 (1999) 295–326.
[7] R.S. Yadav, I. Kuřitka, J. Vilcakova, J. Havlica, L. Kalina, P. Urbánek, M. Machovsky, D. Skoda, M. Masař, M. Holek, Sonochemical synthesis of Gd^{3+} doped $CoFe_2O_4$ spinel ferrite nanoparticles and its physical properties, Ultrason. Sonochem. 40 (2018) 773–783.
[8] M. Maria Lumina Sonia, S. Anand, V. Maria Vinosel, M. Asisi Janifer, S. Pauline, A. Manikandan, Effect of lattice strain on structure, morphology and magneto-dielectric properties of spinel $NiGd_xFe_{2-x}O_4$ ferrite nano-crystallites synthesized by sol-gel route, J. Magn. Magn. Mater. 466 (2018) 238–251.
[9] S.A. Hosseini, Low-cost and eco-friendly viable approach for synthesis of thulium doped copper ferrite nanoparticles using starch, J. Mater. Sci: Mater. Electron. 27 (2016) 7433–7437.
[10] B. Romana, F. Donati, A. Singha, C. Wäckerlin, J. Dreiser, B. Delley, M. Pivetta, S. Rusponi, H. Brune, Magnetic properties of single rare-earth atoms on graphene/Ir (111), Phys. Rev. B 98 (2018) 024412.
[11] L. Zirun, W. Mi, H. Bai, The role of rare–earth dopants in tailoring the magnetism and magnetic anisotropy in Fe_4N, J. Phys. Chem. Solids 116 (2018) 7–14.
[12] J. Liu, F.R. De Boer, P.F. De Châtel, R. Coehoorn, K.H.J. Buschow, On the 4f–3d exchange interaction in intermetallic compounds, J. Magn. Magn. Mater. 132 (1994) 159–179.
[13] S.R. Kulal, R. Shivaji, S.S. Khetre, P.N. Jagdale, V.M. Gurame, D.P. Waghmode, G.B. Kolekar, S.R. Sabale, S.R. Bamane, Synthesis of Dy doped Co–Zn ferrite by sol–gel auto combustion method and its characterization, Mater. Lett. 84 (2012) 169–172.
[14] S.M. Kabbur, S.D. Waghmare, D.Y. Nadargi, S.D. Sartale, R.C. Kambale, U.R. Ghodake, S.S. Suryavanshi, Magnetic interactions and electrical properties of Tb^{3+} substituted NiCuZn ferrites, J. Magn. Magn. Mater. 473 (2019) 99–108.
[15] D. Changwei, G. Xi, T. Zhao, Y. Zhang, Y. Liu, L. Yang, Influence of Er^{3+} substitution on the structural, magnetic, and magnetostrictive properties of cobalt ferrite synthesized from spent Li-ion batteries, Ceram. Int. 44 (2018) 9276–9282.
[16] A. Zubair, Z. Ahmad, A. Mahmood, W.C. Cheong, I. Ali, M.A. Khan, eel Hussain Chughtai, M.N. Ashiq, Structural, morphological and magnetic properties of Eu-doped $CoFe_2O_4$ nano-ferrites, Results Phys. 7 (2017) 3203–3208.
[17] R.N. Mehdi, M. Behpour, A.S. Nasab, M.R. Jeddy, Nanocrystalline Ce-doped copper ferrite: synthesis, characterization, and its photocatalyst application, J. Mater. Sci: Mater. Electron. 27 (2016) 11691–11697.
[18] R. Tholkappiyan, K. Vishista, Influence of lanthanum on the optomagnetic properties of zinc ferrite prepared by combustion method, Phys. B: Condens. Matter 448

(2014) 177–183.
[19] R. Tholkappiyan, K. Vishista, Combustion synthesis of Mg–Er ferrite nanoparticles: cation distribution and structural, optical, and magnetic properties, Mat. Sci. Semicon. Proc. 40 (2015) 631–642.
[20] M.A. Almessiere, A. Demir Korkmaz, Y. Slimani, M. Nawaz, S. Ali, A. Baykal, Magneto-optical properties of rare earth metals substituted Co-Zn spinel nanoferrites, Ceram. Int. 45 (2019) 3449–3458.
[21] K. Elayakumar, A. Dinesh, A. Manikandan, M. Palanivelu, G. Kavitha, S. Prakash, R.T. Kumar, S.K. Jaganathan, A. Baykal, Structural, morphological, enhanced magnetic properties and antibacterial bio-medical activity of rare earth element (REE) cerium (Ce^{3+}) doped $CoFe_2O_4$ nanoparticles, J. Magn. Magn. Mater. 476 (2019) 157–165.
[22] M.F. Valan, A. Manikandan, S.A. Antony, Microwave combustion synthesis and characterization studies of magnetic $Zn_{1-x}Cd_xFe_2O_4$ ($0 \leq x \leq 0.5$) nanoparticles, J. Nanosci. Nanotechnol. 15 (2015) 4543–4551.
[23] M.A. Almessiere, Y. Slimani, S. Güner, M. Nawaz, A. Baykal, F. Aldakheel, S. Akhtar, I. Ercan, İ. Belenli, B. Ozçelik, Magnetic and structural characterization of Nb^{3+} -substituted $CoFe_2O_4$ nanoparticles, Ceram. Int. 45 (2019) 8222–8232.
[24] M.A. Almessiere, Y. Slimani, S. Ali, A. Baykal, I. Ercan, H. Sozeri, Nd^{3+} ion substituted $Co_{1-2x}Ni_xMn_xFe_{2-y}O_4$ nanoparticles: structural, morphological and magnetic investigation, J. Inorg. Organomet. Polym. 29 (2019) 783–791.
[25] Y. Slimani, M.A. Almessiere, M. Nawaz, A. Baykal, S. Akhtar, I. Ercan, I. Belenli, Effect of bimetallic (Ca, Mg) substitution on magneto-optical properties of $NiFe_2O_4$ nanoparticles, Ceram. Int. 45 (2019) 6021–6029.
[26] S.E. Shirsath, M.L. Mane, Y. Yasukawa, X. Liu, A. Morisako, Chemical tuning of structure formation and combustion process in $CoDy_{0.1}Fe_{1.9}O_4$ nanoparticles: influence@pH, J. Nanopart. Res. 15 (2013) 1976.
[27] S.E. Shirsath, M.L. Mane, Y. Yasukawa, X. Liu, A. Morisakoa, Self-ignited high temperature synthesis and enhanced super-exchange interactions of Ho^{3+}–Mn^{2+}–Fe^{3+}–O^{2-} ferromagnetic nanoparticles, Phys. Chem. Chem. Phys. 16 (2014) 2347–2357.
[28] S.E. Shirsath, D. Wang, S.S. Jadhav, M.L. Mane, S. Li, Ferrites obtained by sol-gel method, in: L. Klein, M. Aparicio, A. Jitianu (Eds.), Handbook of Sol-Gel Science and Technology, Springer, Cham, 2018, pp. 695–735.
[29] S.E. Shirsath, X. Liu, Y. Yasukawa, S. Li, A. Morisako, Switching of magnetic easy-axis using crystal orientation for large perpendicular coercivity in $CoFe_2O_4$ thin film, Sci. Rep. 6 (2016) 30074.
[30] A. Manikandan, R. Sridhar, S. Arul Antony, S. Ramakrishna, A simple aloe vera plant-extracted microwave and conventional combustion synthesis: morphological, optical, magnetic and catalytic properties of $CoFe_2O_4$ nanostructures, J. Mol. Struct. 1076 (2014) 188–200.
[31] A. Manikandan, M. Durka, K. Seevakan, S.A. Antony, A novel one-pot combustion synthesis and opto-magnetic properties of magnetically separable spinel $Mn_xMg_{1-x}Fe_2O_4$ ($0.0 \leq x \leq 0.5$) nanophotocatalysts, J. Supercond. Nov Magn. 28 (2015) 1405–1416.
[32] A. Manikandan, E. Hema, M. Durka, K. Seevakan, T. Alagesan, S.A. Antony, Room temperature ferromagnetism of magnetically recyclable photocatalyst of $Cu_{1-x}Mn_xFe_2O_4$-TiO_2 ($0.0 \leq x \leq 0.5$) nanocomposites, J. Supercond. Nov Magn. 28 (2015) 1783–1795.
[33] Y. Slimani, H. Güngüneş, M. Nawaz, A. Manikandan, H.S. El Sayed, M.A. Almessiere, H. Sözeri, S.E. Shirsath, I. Ercan, A. Baykal, Magneto-optical and microstructural properties of spinel cubic copper ferrites with Li-Al co-substitution, Ceram. Int. 44 (2018) 14242–14250.
[34] M.A. Almessiere, Y. Slimani, A.D. Korkmaz, S. Guner, M. Sertkol, Sagar E. Shirsath, A. Baykal, Structural optical and magnetic properties of Tm^{3+} substituted cobalt spinel ferrites synthesized via sonochemical approach, Ultrason. Sonochem. 54 (2019) 1–10.
[35] J. Tauc, R. Grigorovici, A. Vancu, Optical properties and electronic structure of amorphous germanium, Phys. Status Solidi 15 (1966) 627–637.
[36] A. Baykal, S. Guner, H. Gungunes, K.M. Batoo, Md Amir, A. Manikandan, Magneto optical properties and hyperfine interactions of Cr^{3+} ion substituted copper ferrite nanoparticles, J. Inorg. Organomet. Polym. 28 (2018) 2533–2544.
[37] A. Baykal, S. Esir, A. Demir, S. Güner, Magnetic and optical properties of $Cu_{1-x}Zn_xFe_2O_4$ nanoparticles dispersed in a silica matrix by a sol-gel auto-combustion method, Ceram. Int. 41 (2015) 231–239.
[38] A. Manikandan, M. Durka, S. Arul Antony, A novel synthesis, structural, morphological, and opto-magnetic characterizations of magnetically separable spinel $Co_xMn_{1-x}Fe_2O_4$ ($0 \leq x \leq 1$) Nano-catalysts, J. Supercond. Nov. Magn. 27 (2014) 2841–2857.
[39] E. Hema, A. Manikandan, P. Karthika, S. Arul Antony, B.R. Venkatraman, A novel synthesis of Zn^{2+}-doped $CoFe_2O_4$ spinel nanoparticles: structural, morphological, opto-magnetic and catalytic properties, J. Supercond. Nov. Magn. 28 (2015) 2539–2552.
[40] T.E.P. Alves, H.V.S. Pessoni, A. Franco Jr, The effect of Y^{3+} substitution on the structural, optical band-gap, and magnetic properties of Cobalt ferrite nanoparticles, Phys. Chem. Chem. Phys. 19 (2017) 16395.
[41] S. Supriya, S. Kumar, M. Kar, band gap engineering of Z substituted cobalt ferrite for optoelectronic applications, IEEE, Nanotechnology Material and Devices Conference, (2017) October 2–4 Singapore.
[42] A. Manikandan, M. Durka, S.A. Antony, Role of Mn^{2+} doping on structural, morphological, and opto-magnetic properties of spinel $Mn_xCo_{1-x}Fe_2O_4$ ($x = 0.0, 0.1, 0.2, 0.3, 0.4$, and 0.5) nanocatalysts, J. Supercond. Nov. Magn. 28 (2015) 2047–2058.
[43] M. Saha, S. Mukherjee, A. Gayen, Microstructure, optical and magnetic properties of inverse spinel $CoFe_2O_4$ synthesized by microemulsion process assisted by CTAB and AOT, J. Aust. Ceram. Soc. 52 (2016) 150–162.
[44] J.L.O. Quinonez, U. Pal, M.S. Villanueva, Structural, magnetic, and catalytic evaluation of spinel Co, Ni, and Co-Ni ferrite nanoparticles fabricated by low-temperature solution combustion process, ACS Omega 3 (2018) 14986–15001.
[45] M.A. Almessiere, Y. Slimani, S. Güner, M. Nawaz, A. Baykal, F. Aldakheel, S. Akhtar, I. Ercan, İ. Belenli, B. Ozçelik, Magnetic and structural characterization of Nb^{3+}-substituted $CoFe_2O_4$ nanoparticles, Ceram. Int. 45 (2019) 8222–8232.
[46] E.C. Stoner, E. Wohlfarth, A mechanism of magnetic hysteresis in heterogeneous alloys, Philos. Trans. Royal Soc. London Series A Math. Phys. Sci. 240 (1948) 599–642.
[47] M.A. Almessiere, Y. Slimani, H.S. El Sayed, A. Baykal, Morphology and magnetic traits of strontium nanohexaferrites: effects of manganese/yttrium co-substitution, J. Rare Earths (2019), https://doi.org/10.1016/j.jre.2018.1009.1014.
[48] M. Almessiere, Y. Slimani, H.S. El Sayed, A. Baykal, Ca^{2+} and Mg^{2+} incorporated barium hexaferrites: structural and magnetic properties, J. Sol-Gel Sci. Technol. 88 (2018) 628–638.
[49] S. Laurent, D. Forge, M. Port, A. Roch, C. Robic, L.V. Elst, R.N. Muller, Magnetic iron oxide nanoparticles: synthesis, stabilization, vectorization, physicochemical characterizations, and biological applications, Chem. Rev. 108 (2008) 2064–2110.
[50] L. Almásy, D. Creanga, C. Nadejde, L. Rosta, E. Pomjakushina, M. Ursache-Oprisan, Wet milling versus co-precipitation in magnetite ferrofluid preparation, J. Serb. Chem. Soc. 80 (2015) 367–376.
[51] A. Nairan, M. Khan, U. Khan, M. Iqbal, S. Riaz, S. Naseem, Temperature-dependent magnetic response of antiferromagnetic doping in cobalt ferrite nanostructures, Nanomaterials 6 (2016) 73.
[52] P.J. Wasilewski, Magnetic hysteresis in natural materials, Earth Planet. Sci. Lett. 20 (1973) 67–74.
[53] Q. Gao, G. Hong, J. Ni, W. Wang, J. Tang, J. He, Uniaxial anisotropy and ovel magnetic behaviours of $CoFe_2O_4$ nanoparticles prepared in a magnetic field, J. Appl. Phys. 105 (2009) 105.
[54] S. Heisz, G. Hilscher, The origin of graduated demagnetization curves of NdFeB magnets, J. Magn. Magn. Mater. 67 (1987) 20–28.
[55] A.P. Roberts, Y. Cui, K.L. Verosub, Wasp-waisted hysteresis loops: mineral magnetic characteristics and discrimination of components in mixed magnetic systems, J. Geophys. Res. 100 (1995) 17909–17924.
[56] M. Almessiere, Y. Slimani, N. Tashkandi, A. Baykal, M. Saraç, A. Trukhanov, İ. Ercan, İ. Belenli, B. Ozçelik, The effect of Nb substitution on magnetic properties of $BaFe_{12}O_{19}$ nanohexaferrites, Ceram. Int. 45 (2019) 1691–1697.
[57] M. Almessiere, Y. Slimani, H. Gungunes, A. Manikandan, A. Baykal, Investigation of the effects of Tm^{3+} on the structural, microstructural, optical, and magnetic properties of Sr hexaferrites, Results Phys. 13 (2019) 102166.
[58] Y. Melikhov, J.E. Snyder, D.C. Jiles, A.P. Ring, J.A. Paulsen, C.C.H. Lo, K.W. Dennis, Temperature dependence of magnetic anisotropy in Mn-substituted cobalt ferrite, J. Appl. Phys. 99 (2006).
[59] Y. Koseoglu, A. Baykal, F. Gozuak, H. Kavas, Structural and magnetic properties of $Co_xZn_{1-x}Fe_2O_4$ nanocrystals synthesized by microwave method, Polyhedron 28 (2009) 2887–2892.
[60] G.V. Duong, N. Hanh, D.V. Linh, R. Groessinger, P. Weinberger, E. Schafler, M. Zehetbauer, Monodispersed nanocrystalline $Co_{1-x}Zn_xFe_2O_4$ particles by forced hydrolysis: synthesis and characterization, J. Magn. Magn. Mater. 311 (2007) 46–50.
[61] M. Amir, H. Gungunes, Y. Slimani, N. Tashkandi, H. El Sayed, F. Aldakheel, M. Sertkol, H. Sozeri, A. Manikandan, I. Ercan, Mössbauer studies and magnetic properties of cubic $CuFe_2O_4$ nanoparticles, J. Supercond. Nov Magn. (2018), https://doi.org/10.1007/s10948-018-4733-5.
[62] M. Almessiere, Y. Slimani, S. Güner, A. Baykal, I. Ercan, Effect of dysprosium substitution on magnetic and structural properties of $NiFe_2O_4$nanoparticles, J. Rare Earths (2019), https://doi.org/10.1016/j.jre.2018.10.009.
[63] R.D. Shannon, Revised effective ionic radii and systematic studies of interatomic distances in halides and chalcogenides, Acta Crystallogr. A 32 (1976) 751–767.
[64] Y. Slimani, M.A. Almessiere, S. Güner, N.A. Tashkandi, A. Baykal, M.F. Sarac, M. Nawaz, I. Ercan, Calcination effect on the magneto-optical properties of vanadium substituted $NiFe_2O_4$ nanoferrites, J. Mater. Sci.: Mater. Electron. (2019), https://doi.org/10.1007/s10854-019-01243-x.
[65] M.A. Almessiere, Y. Slimani, S. Ali, A. Baykal, I. Ercan, H. Sozeri, Nd^{3+} ion-substituted $Co_{1-2x}Ni_xMn_xFe_{2-y}Nd_yO_4$ nanoparticles: structural, morphological, and magnetic investigations, J. Inorg. Organomet. Polym. (2018), https://doi.org/10.1007/s10904-018-1052-z.
[66] M.A. Almessiere, Y. Slimani, M. Sertkol, M. Nawaz, A. Baykal, I. Ercan, The impact of Zr substituted Sr hexaferrite: investigation on structure, optic and magnetic properties, Results Phys. 13 (2019) 102244.